

High-fat overfeeding impairs peripheral glucose metabolism and muscle microvascular eNOS Ser¹¹⁷⁷ phosphorylation

Siôn A. Parry^{1*}, Mark C. Turner^{1,2}, Rachel M. Woods¹, Lewis J. James¹, Richard A. Ferguson¹, Matthew Cocks³, Katie L. Whytock³, Juliette A. Strauss³, Sam O. Shepherd³, Anton J.M. Wagenmakers³, Gerrit van Hall^{4,5}, Carl J. Hulston¹

¹School of Sport, Exercise & Health Sciences, Loughborough University, Loughborough, UK

²University Hospitals of Leicester NHS Trust, Infirmary Square, Leicester, UK

³School of Sport & Exercise Sciences, Liverpool John Moores University, Liverpool, UK

⁴Clinical Metabolomics Core Facility, Department of Clinical Biochemistry, Rigshospitalet, Copenhagen, Denmark

⁵Department of Biomedical Sciences, University of Copenhagen, Copenhagen, Denmark

*Current address: Oxford Centre for Diabetes, Endocrinology and Metabolism, University of Oxford, Churchill Hospital, Oxford, UK

ORCID:

Carl Hulston

0000-0002-5375-1161

Clinical trials registration number: NCT03879187

Address for correspondence

Carl J. Hulston, PhD

School of Sport, Exercise & Health Sciences

Loughborough University

Loughborough

LE11 3TU

Telephone: +44 1509 226 449

Email: c.j.hulston@lboro.ac.uk

Financial support: The research was funded by the National Institute for Health Research (NIHR) Leicester Biomedical Research Centre. The views expressed are those of the authors and not necessarily those of the NHS, the NIHR or the Department of Health and Social Care.

Disclosure summary: The authors have nothing to disclose.

Abstract

Context: The mechanisms responsible for dietary fat-induced insulin resistance of skeletal muscle and its microvasculature are only partially understood.

Objective: To determine the impact of high-fat overfeeding on postprandial glucose fluxes, muscle insulin signaling, and muscle microvascular eNOS content and activation.

Design: Fifteen non-obese volunteers consumed a high-fat (64%) high-energy (+47%) diet for 7 days. Experiments were performed before and after the diet. Stable isotope tracers were used to determine glucose fluxes in response to carbohydrate plus protein ingestion. Muscle insulin signaling was determined as well as the content and activation state of muscle microvascular eNOS.

Results: High-fat overfeeding impaired postprandial glycemic control as demonstrated by higher concentrations of glucose (+11%; $P = 0.004$) and insulin (+19%; $P = 0.035$). Carbohydrate plus protein ingestion suppressed endogenous glucose production to a similar extent before and after the diet. Conversely, high-fat overfeeding reduced whole body glucose clearance (-16%; $P = 0.021$) and peripheral insulin sensitivity (-26%; $P = 0.006$). This occurred despite only minor alterations in skeletal muscle insulin signaling. High-fat overfeeding reduced eNOS content in terminal arterioles ($P = 0.017$) and abolished the increase in eNOS Ser¹¹⁷⁷ phosphorylation that was seen after carbohydrate plus protein ingestion.

Conclusion: High-fat overfeeding impaired whole-body glycemic control due to reduced glucose clearance, not elevated endogenous glucose production. The finding that high-fat overfeeding abolished insulin-mediated eNOS Ser¹¹⁷⁷ phosphorylation in the terminal arterioles suggests that impairments in the vasodilatory capacity of the skeletal muscle microvasculature may contribute to early dietary fat-induced impairments in glycemic control.

Key words: High-fat diet, glucose kinetics, skeletal muscle, insulin signaling, eNOS

Précis

Healthy volunteers consumed a high-fat diet for 7 days. The diet impaired peripheral glucose clearance and abolished insulin-stimulated eNOS phosphorylation within the muscle microvasculature.

Accepted Manuscript

Introduction

Excessive food intake and physical inactivity have driven the obesity epidemic, with obesity being a major risk factor for the development of insulin resistance and the metabolic syndrome¹. However, just a few days of excessive dietary fat intake can impair insulin action and glycemic control in healthy non-obese individuals²⁻⁴. Understanding these early responses may provide insight into metabolic disease progression.

Impairments in glycemic control may be mediated by the inability of insulin to suppress endogenous glucose production (EGP) in the liver and/or a reduction in insulin-stimulated glucose uptake by peripheral tissues⁵. The tissue-specific contributions to dietary fat-induced impairments in glycemic control are only partially understood. One study reported a reduction in hepatic insulin sensitivity and an increase in basal EGP in healthy men subjected to 5-days of high-fat overfeeding⁶. In that study, high-fat overfeeding had no effect on insulin-stimulated glucose disposal, suggesting that changes in hepatic glucose metabolism precede that of peripheral impairments. In contrast, another study reported a reduction in insulin-stimulated leg glucose uptake after 3-days of high-fat overfeeding, but no change in hepatic insulin sensitivity or EGP at baseline or following insulin administration³. Each of these studies utilized the hyperinsulinemic-euglycemic clamp, which, although useful, can be criticized due to its failure to mimic postprandial conditions. Under clamp conditions, skeletal muscle is responsible for 70-80% of glucose disposal, and EGP is completely suppressed. Following glucose ingestion, splanchnic extraction and skeletal muscle glucose uptake make roughly equal contributions to meal-derived glucose disposal (~30% each), and EGP is only partially suppressed (50-60% decrease)⁷⁻¹⁰. Thus, the processes governing postprandial glycemic control are more dynamic/ complex than that of clamps. Moreover, as the normal route for glucose entry into the body is via the gastrointestinal tract, it is necessary to determine the

impact of high-fat overfeeding on postprandial glucose fluxes (i.e., meal-derived glucose entry into the circulation, suppression of EGP, and stimulation of glucose disposal), which can be achieved through the use of dual-glucose tracers ^{7,10}.

As well as the classical actions of insulin on the myocyte, recent work has established a possible role for the skeletal muscle microvasculature in insulin-mediated glucose disposal ¹¹. Physiological doses of insulin have been shown to increase skeletal muscle perfusion ¹²⁻¹⁴. Inhibition of this hemodynamic action by L-NAME (N(ω)-nitro-L-arginine-methyl ester) or L-NMMA (NG-monomethyl-L-arginine acetate) has been shown to reduce skeletal muscle glucose uptake ¹⁵⁻¹⁷. Alternatively, it has been shown that L-NAME administration can impair glycemic control through inhibition of insulin secretion without changes in peripheral insulin sensitivity ¹⁸, and another study reported that L-NMMA administration prevented vasodilation during insulin/glucose infusion but did not alter whole body glucose uptake ¹⁹. Thus, the role of the skeletal muscle microvasculature in insulin-mediated glucose disposal requires clarification. Animal studies suggest that impairments to insulin's microvascular action could be a key early event in the development of insulin resistance in response to a high fat diet ²⁰⁻²². Importantly, the effect of insulin on the microvasculature is dependent on nitric oxide (NO) synthesized in the endothelium of terminal arterioles. Terminal arterioles regulate the blood flow in microvascular units (MVUs), which are the smallest functional elements to adjust muscle blood flow in response to physiological signals and metabolic demands of the muscle fibers ²³. Each terminal arteriole delivers blood to ± 20 capillaries ²³. Increases in insulin following meal ingestion activate eNOS by means of Ser¹¹⁷⁷ phosphorylation. This leads to the production of NO, relaxation of the smooth muscle layer and vasodilation of the terminal arterioles, thereby increasing blood flow in the MVU's ²⁴. The content of NAD(P)H oxidase in the endothelial layer of the terminal arterioles may reduce NO bioavailability, and therefore

microvascular perfusion of the muscle, through NO scavenging by superoxide anions ^{25,26}. Despite the potential for impaired microvascular perfusion playing a role in lipid-induced insulin resistance, no studies have investigated the protein content and activation state of eNOS and NAD(P)H oxidase in response to a high fat diet.

The present study determined the role of EGP (primarily hepatic), oral glucose appearance, and whole-body glucose clearance in dysregulation of glycemic control after 7 days of high-fat overfeeding. To this end, we used stable isotope tracers to assess glucose fluxes in response to acute oral ingestion of an insulinotropic carbohydrate-protein mixture. We also determined the phosphorylation (activation) of key proteins involved in skeletal muscle insulin signaling as well as the protein content and activation state of eNOS and NADP(H) oxidase. We hypothesized that high-fat overfeeding would impair glucose clearance, not endogenous glucose production. We also hypothesized that high-fat overfeeding would impair insulin-stimulated eNOS Ser¹¹⁷⁷ phosphorylation, thereby identifying the muscle microvasculature as an early possible cause of dietary fat-induced insulin resistance.

Methods

Participants

Fifteen individuals (13 males/ 2 females) age 24 ± 1 y, height 176.1 ± 2.1 cm, body mass 77.15 ± 3.07 kg, and body mass index (BMI) 24.8 ± 0.6 kg/m² participated in this study. Participants were physically active, non-smokers, with no diagnosis of cardiovascular or metabolic disease, not taking any medication, and weight stable for ≥ 3 months. The study was approved by the local ethics committee and every participant provided written informed consent. Experimental trials were conducted from March 2015 to August 2016. Analysis was completed by May 2018. The study was registered at ClinicalTrials.gov (identifier: NCT03879187).

Pre-testing

Participants attended the laboratory for assessment of anthropometric characteristics (height, body mass and BMI). This information was used to estimate resting energy expenditure (REE)²⁷. A standard correction for physical activity (1.6 and 1.7 times REE for females and males, respectively) was applied to estimate total daily energy requirements. This information was used to determine individual energy intakes for the diet intervention.

Experimental design

One-week after the pre-testing visit, participants returned to the laboratory to undergo metabolic testing. Participants then consumed a high-fat, high-energy diet for 7 days. The diet provided 4749 ± 181 kcal per day, with 188 ± 8 g [16% total energy (TE)] protein, 237 ± 8 g [20% TE] carbohydrate, and 333 ± 14 g [64% TE] fat intake. All foods were purchased and prepared by the research team. Participants were instructed to eat everything that was provided, not to eat any additional food, and to return any uneaten items so that diet values could be adjusted if necessary. All participants were informed about the importance of strict diet

adherence. Adherence was checked by daily interviews that were conducted when participants collected their food bundles. A second metabolic testing session was conducted the morning after completing the diet.

Experimental protocol

Participants reported to the laboratory in the morning after an overnight fast (≥ 12 h), having refrained from strenuous physical activity for ≥ 48 h. After voiding and being weighed, a Teflon catheter (Venflon; Becton, Dickinson, Plymouth, UK) was inserted into an antecubital vein of each arm to allow blood sampling and isotope infusion. A baseline blood sample (10 mL) was obtained before a primed constant infusion of [6,6- $^2\text{H}_2$]glucose was initiated and continued for the duration of the experiment. Blood samples were divided between tubes containing EDTA or a clotting catalyst (Sarstedt, Leicester, UK). Further blood samples were obtained 90, 105 and 120 min into the infusion (referred to as $t = -30, -15$ and 0 min in results/ figures). Biopsies were obtained from the *vastus lateralis* under local anesthesia (Lidocaine 10 mg/mL) using a 5-mm Bergström needle, modified for use with manual suction. Two sections of muscle tissue were blotted free of blood, snap-frozen in liquid nitrogen, and stored at -80°C . A third section of muscle tissue was mounted in Tissue-Tek OCT (Sakura Finetek UK Ltd, Thatcham, UK) and frozen in liquid nitrogen-cooled isopentane for cryo-sectioning and immunofluorescence microscopy. Participants then consumed a carbohydrate plus protein solution. Further blood samples were obtained at 15, 30, 45, 60, 90- and 120-min post-ingestion, and additional muscle biopsies were obtained at 30- and 120-min post-ingestion.

Two participants did not undergo the muscle biopsy procedure, so measurements of skeletal muscle insulin signaling are reported for $n = 13$. Data for immunofluorescence microscopy are reported for $n = 12$ and data for muscle glycogen are reported for $n = 11$ due to tissue quantity

limitations. Data for glucose kinetics are reported for n = 14 due to a technical issue with the preparation of isotopes for one of the trials. All other data reported for n = 15.

Carbohydrate plus protein beverage

The test beverage was a 12.5% glucose solution (48.4 g glucose plus 1.6 g [U-¹³C]glucose in 400 mL of water) with 15 g whey protein (UltraWhey 90; Volac, Hertfordshire, UK). Whey protein was added to the solution as most meals will contain protein and to increase the insulinotropic effect of the beverage.

Blood analyses

Plasma samples were analyzed for triacylglycerol (TAG), total cholesterol, high-density lipoprotein cholesterol (HDL), low-density lipoprotein cholesterol (LDL) (Horiba Medical, Northampton, UK) and non-esterified fatty acids (NEFA; Randox, County Antrim, UK) using a semi-automated analyzer (Pentra 400; Horiba Medical, Northampton, UK). Serum insulin was determined using ELISA (EIA-2935; DRG instruments GmbH, Marburg, Germany). Plasma glucose concentration and enrichment was determined using liquid chromatography-tandem mass spectrometry (LC-MS/MS) as previously described ²⁸.

Muscle analyses

Glycogen analysis

Glycogen content was determined as glycosyl units after acid hydrolysis and was measured spectrophotometrically. The coefficient of variation for glycogen determination was 7-11% (determined on multiple preparations from 3 separate biopsies).

Western blotting

To investigate skeletal muscle insulin signaling, commercially available antibodies were used to determine the phosphorylation of key proteins (Akt Ser⁴⁷³ [Cell Signaling #4060], Akt Thr³⁰⁸ [Cell Signaling #13038], AS160 Ser⁵⁸⁸ [Cell Signaling #8730], and AS160 Thr⁶⁴² [Cell Signaling #8881] by SDS-PAGE and Western blotting as previously described ²⁹

Quantitative immunofluorescence

Details of the specific quantification techniques can be found below, and all techniques have been described in detail previously, including antibody specificity experiments ^{30,31}. All techniques used frozen muscle biopsy samples cryosectioned to a thickness of 5 µm, mounted onto uncoated glass microscope slides so that transverse orientated samples could be used for analysis. Two sections from each condition (pre and post high-fat overfeeding; 0 and 30 min) within a participant were placed on the same slide and analysis was performed in duplicate (two slides).

Sections were fixed in acetone and ethanol (3:1). For assessment of eNOS Ser¹¹⁷⁷/eNOS ratio, sections were triple stained with antibodies against eNOS (Transduction Laboratories, Lexington, KY, USA), eNOS Ser¹¹⁷⁷ (Cell Signaling Technology, Beverly, MA, USA) and anti-α smooth muscle actin (αSMA; Abcam, Cambridge, UK). For assessment of NOX2 and p47phox content, sections were double stained with either NOX2 or p47phox (kind gift from Prof Mark Quinn, Montana State University) and anti-αSMA. All sections were then incubated with appropriate secondary antibodies (Invitrogen, Paisley, UK) in combination with the endothelial marker Ulex Europaeus-FITC conjugated (UEA-I-FITC; Sigma-Aldrich, UK).

Images were acquired using an inverted confocal microscope (Zeiss LSM-710, Carl Zeiss, Germany) with a 40x NA oil immersion objective. Alexa Fluor 405 was excited using the 405 nm line of the diode laser and detected with 371–422 nm emission. FITC fluorescence was excited with a 488 nm line of the argon laser and detected with 493–559 nm emission. Alexa Fluor 546 and 633 fluorophores were excited with 543 nm and 633 nm lines of the helium–neon laser and 548–623 nm and 638–747 nm emission, respectively. Identical settings were used for all image capture within each participant.

All image analysis was performed using ImagePro Plus 5.1 (Media Cybernetics Inc, Bethesda, MD, USA). Blood vessels were divided into either capillaries or arterioles using the α SMA image. The endothelial (UEA-I-FITC) outline was then overlaid onto the corresponding vascular enzyme image. Mean fluorescence intensity of the vascular enzyme signal was then quantified within the endothelial specific area. Diameter of the arterioles was determined on calibrated images. Vessels larger than 20 μ m in diameter were excluded to remove 3rd and 4th order arterioles³² from the analysis. As eNOS and eNOS Ser¹¹⁷⁷ phosphorylation had been stained on the same sections it was possible to establish eNOS Ser¹¹⁷⁷/eNOS ratio on an individual vessel basis, as the same endothelial outline could be placed over both eNOS and eNOS Ser¹¹⁷⁷ images. The researcher was blinded to condition during imaging and analysis, and all analysis was conducted by the same researcher. 6 ± 1 arterioles and 139 ± 11 capillaries were assessed per participant for eNOS content and eNOS Ser¹¹⁷⁷ phosphorylation. 8 ± 1 arterioles and 148 ± 11 capillaries were assessed per participant for NOX2 content. 8 ± 1 arterioles and 154 ± 14 capillaries were assessed per participant for p47phox content.

Calculations

Tracer calculations were performed using a non-steady state, single-pool model as previously described³³. Peripheral insulin sensitivity was calculated as the mean glucose clearance rate during the 2 h postprandial period divided by the mean serum insulin concentration over the same period^{34,35}. Homeostatic model assessment of insulin resistance (HOMA-IR) was calculated as described by³⁶. Area under the curve (AUC) was calculated using the trapezoidal rule with zero as the baseline.

Statistics

All data are presented as means \pm standard error of the mean (SEM). A Shapiro-Wilk test was performed to test for normal distribution. Statistical analysis was performed using SPSS v23 for windows. Paired t-tests were used to make pre to post high-fat overfeeding comparisons where appropriate. All remaining data were compared using a two-way (trial x time) RM ANOVA, followed with Bonferroni-adjusted *post-hoc* t-tests where appropriate. Statistical significance was set at $p < 0.05$.

Results

Body mass and fasting blood parameters

The effect of high-fat overfeeding on body mass and fasting blood parameters is shown in Table 1. High-fat overfeeding increased body mass, plasma glucose, serum insulin, HOMA-IR, total cholesterol and HDL cholesterol. LDL cholesterol was unaffected by the diet, whereas TAG and NEFA decreased.

Postprandial plasma glucose and serum insulin

Plasma glucose and serum insulin increased in response to carbohydrate plus protein ingestion, peaking at 30-45 min (Figure 1A and 1B, respectively). There was a main effect of trial ($P = 0.004$) and a trial x time interaction ($P = 0.012$) for plasma glucose (Figure 1A), with plasma glucose at 30- and 45-min time points being higher after high-fat overfeeding than before. Postprandial plasma glucose AUC (0 – 120 min) increased by 11% after high-fat overfeeding (596 ± 23 mmol/L per 120 min before vs. 663 ± 19 mmol/L per 120 min after; $P = 0.004$). A main effect of trial ($P = 0.034$) and a trial x time interaction ($P = 0.009$) were also evident for serum insulin (Figure 1B), with serum insulin at the 45-min time point being higher after high-fat overfeeding than before. Postprandial serum insulin AUC increased by 19% after high-fat overfeeding ($34,164 \pm 4,525$ pmol/L per 120 min before vs. $40,715 \pm 3,143$ pmol/L per 120 min after; $P = 0.035$).

EGP, oral glucose appearance, and whole-body glucose clearance

There was a trial x time interaction for EGP ($P = 0.009$; Figure 2A). High-fat overfeeding reduced EGP during fasting and early postprandial measurements, and carbohydrate plus protein ingestion suppressed EGP to a similar extent before and after high-fat overfeeding.

Thus, alterations in EGP did not contribute to elevated glucose concentrations. Oral glucose appearance was unaffected by high-fat overfeeding, although there was a tendency for a trial x time interaction ($P = 0.062$; Figure 2B). Lastly, there was a main effect of trial ($P = 0.025$) for whole body glucose clearance, with high-fat overfeeding resulting in reduced glucose clearance rate (Figure 2C). When calculated for the entire 2 h oral glucose challenge, high-fat overfeeding reduced time-averaged whole-body glucose clearance rate by 16% (3.2 ± 0.2 mL/kg/min post vs. 3.8 ± 0.2 mL/kg/min pre; $P = 0.021$). Thus, elevated glucose concentrations observed after high-fat overfeeding were due to reduced glucose disposal and not increased liver glucose output.

Peripheral insulin sensitivity

Peripheral insulin sensitivity decreased by 26% after high-fat overfeeding (10.4 ± 1.7 mL/kg/min/nmol/L post vs. 14.2 ± 1.6 mL/kg/min/nmol/L pre; $P = 0.006$).

Skeletal muscle insulin signaling

The phosphorylation of key intermediates of the insulin signaling cascade is shown in Figure 3. Phosphorylation of Akt Ser⁴⁷³, Akt Thr³⁰⁸, AS160 Ser⁵⁸⁸ and AS160 Thr⁶⁴² increased from 0 to 30 min after carbohydrate plus protein ingestion ($P < 0.05$). This response was not affected by high-fat overfeeding. Phosphorylation of Akt Ser⁴⁷³, Akt Thr³⁰⁸ and AS160 Thr⁶⁴² decreased from 30 to 120 min. However, phosphorylation of AS160 Thr⁶⁴² was higher at 120 min than at 0 min. There was a trial x time interaction for AS160 Ser⁵⁸⁸ ($P = 0.042$). Before high-fat overfeeding, phosphorylation of AS160 Ser⁵⁸⁸ remained elevated 120 min after carbohydrate plus protein ingestion. After high-fat overfeeding, phosphorylation of AS160 Ser⁵⁸⁸ returned to baseline at 120 min.

Muscle glycogen

High-fat overfeeding had no effect on muscle glycogen content. Fasting muscle glycogen content was 430 ± 37 mmol/kg dm before high-fat overfeeding and 398 ± 28 mmol/kg dm after. Carbohydrate plus protein ingestion did not affect muscle glycogen content either, such that values at 120 min were comparable to those seen at 0 min.

Total and phosphorylated eNOS

eNOS content of terminal arterioles and capillaries is shown in Figure 4. High-fat overfeeding reduced eNOS content within terminal arterioles by 6% ($P = 0.017$), whereas high-fat overfeeding did not affect eNOS content within the capillaries ($p = 0.197$). High-fat overfeeding also altered eNOS phosphorylation (Figure 5). Before high-fat overfeeding, carbohydrate plus protein ingestion increased eNOS Ser¹¹⁷⁷ phosphorylation within terminal arterioles by 11%. This effect was no longer present after high-fat overfeeding (Figure 5C; trial x time interaction, $P = 0.007$). A near identical response was observed when eNOS Ser¹¹⁷⁷ phosphorylation was normalized to eNOS content, with nutrient intake resulting in an 8% increase in eNOS Ser¹¹⁷⁷/eNOS before high-fat overfeeding but no increase after (Figure 5D; trial x time interaction, $P = 0.039$). A similar response was observed within the capillaries, with a nutrient-stimulated 7% increase in eNOS Ser¹¹⁷⁷/eNOS before high-fat overfeeding but no increase after (Figure 5D; trial x time interaction, $P = 0.013$).

NAD(P)H oxidase

The protein content of the NAD(P)H oxidase subunits NOX2 (enzymatic subunit) and p47phox (main regulator subunit) was determined within terminal arterioles and capillaries. High-fat overfeeding had no effect on the content of either subunit of the NAD(P)H oxidase complex (Figure 6).

Discussion

The tissue-specific changes in glucose metabolism that underpin dietary fat-induced impairments in glycemic control are not fully understood. The main observation of this study was that 7 days of high-fat overfeeding led to an increase in postprandial glucose concentration that was attributable to a reduction in whole body glucose clearance, not elevated EGP. This suggests that peripheral tissue (such as skeletal muscle) is the primary site of early lipid-induced impairments in glucose metabolism. Despite this, we observed little to no change in skeletal muscle insulin signaling, suggesting that mechanisms other than impaired insulin signaling are responsible for the reduction in glucose clearance. Notably, high-fat overfeeding abolished insulin-mediated eNOS Ser¹¹⁷⁷ phosphorylation in skeletal muscle terminal arterioles, suggesting that reduced NO production leading to reduced perfusion of skeletal muscle in response to insulin may be involved in mediating impaired glucose clearance in response to 7 days of high-fat overfeeding.

High-fat overfeeding has frequently been applied in animal studies aiming to better understand the mechanisms leading to obesity and insulin resistance. These studies are consistent in suggesting that hepatic insulin resistance precedes that of skeletal muscle insulin resistance³⁷⁻⁴⁰. Human research has produced equivocal findings, with both the liver⁶ and skeletal muscle³ suggested as the primary site of altered glucose metabolism. Brons *et al.*⁶ reported a 26% increase in basal EGP after high-fat overfeeding that resulted in a 0.46 mmol/L increase in fasting glucose. In contrast, we observed a 7% decrease in basal EGP despite a significant increase in fasting plasma glucose. The reason for this discrepancy is unclear, as both the subject characteristics and the diet intervention were similar between the two studies. Balancing EGP with exogenous glucose supply is an essential component of glycemic control,

and one that is impaired in type 2 diabetes ⁴¹. We found that the ability to suppress EGP in response to carbohydrate plus protein ingestion was adequately maintained following high-fat overfeeding. It is not possible to consider this observation in the context of the data from Brons *et al.* ⁶ as their use of a hyperinsulinemic-euglycemic clamp led to the complete suppression of EGP, regardless of diet. However, individuals with prediabetes also retain adequate suppression of EGP despite postprandial hyperglycemia relative to individuals with normal glucose tolerance ⁴². Thus, in the early stages of insulin resistance it seems that alterations in hepatic glucose metabolism do not contribute to whole body impairments in glycemic control. We also determined oral glucose appearance rate and found that it was not affected by 7 days of high-fat overfeeding. The proportion of ingested glucose reaching the systemic circulation after 2 h was 57% before high-fat overfeeding and 53% after, which is comparable to that reported for healthy individuals ¹⁰.

High-fat overfeeding caused a 16% decrease in whole body glucose clearance, which is in close agreement with the 20% decrease in leg glucose uptake recently reported after 3 days of increased fat intake ³. This is also comparable to the physiology of prediabetes, where postprandial hyperglycemia has been attributed to reduced glucose clearance, not increased oral glucose appearance or increased EGP ⁴². Skeletal muscle is a major contributor to insulin-stimulated glucose disposal both under clamp conditions ⁴³ and following glucose ingestion ⁷⁻¹⁰. We therefore determined the effect of high-fat overfeeding on components of the skeletal muscle insulin signaling cascade. We focused our attention on Akt and the 160-kDa Akt substrate (AS160; also known as TBC1D4); the latter has been identified as the most proximal component of the insulin-signaling cascade linked to GLUT4 translocation ⁴⁴⁻⁴⁶ and an important regulator of insulin-stimulated skeletal muscle glucose uptake ⁴⁷. As insulin-stimulated AS160 activation is impaired in skeletal muscle of type 2 diabetics ⁴⁸, this protein

could play a role in dietary lipid-induced impairments in muscle glucose uptake. In the present study, carbohydrate plus protein intake led to a robust increase in the phosphorylation of Akt Ser⁴⁷³ and Thr³⁰⁸ as well as AS160 Ser⁵⁸⁸ and Thr⁶⁴². However, high-fat overfeeding had little to no effect on basal or carbohydrate plus protein-stimulated phosphorylation of either protein. Others have reported similar. For example, acute lipid-heparin infusion was found to decrease glucose disposal by 50%, without changes in Akt Ser⁴⁷³ phosphorylation⁴⁹, and high-fat overfeeding reduced insulin-stimulated leg glucose uptake independent of changes in Akt Thr³⁰⁸ or AS160 PAS phosphorylation³. Collectively, these findings suggest that alterations in Akt/AS160 activation do not play a role in early lipid-induced impairments in glucose disposal, at least in response to high fat food intake for up to 7 days.

In the study by Lundsgaard *et al.*³, reduced leg glucose uptake was attributed to increased PDH-E1 α Ser³⁰⁰ phosphorylation and a downregulation in oxidative glucose disposal. Insulin-induced GLUT4 translocation in combination with activation of PDH plays a key role in determining insulin-stimulated glucose oxidation⁵⁰, which is an important route of glucose disposal⁵¹. It is well known that high-fat feeding inhibits PDH and reduces carbohydrate oxidation both at rest and during exercise^{52,53}. Thus, whilst we do not have data on PDH activity or whole-body carbohydrate oxidation, it is likely that high-fat overfeeding inhibited PDH and reduced oxidative glucose disposal, which could partially explain the reduction in glucose clearance. Glucose taken up by skeletal muscle can also be diverted to glycogen storage. In the present study, basal muscle glycogen was unaffected by high-fat overfeeding, suggesting that the amount of carbohydrate provided was enough to maintain glycogen synthesis rates in the high fat feeding period. Additionally, acute carbohydrate plus protein ingestion did not stimulate glycogen synthesis either before or after high-fat overfeeding,

supporting the idea that ingested carbohydrate may have been partitioned towards oxidative disposal.

High-fat overfeeding caused a small but significant 6% reduction in eNOS content in terminal arterioles. Perhaps more importantly, high-fat overfeeding abolished the increase in eNOS Ser¹¹⁷⁷ phosphorylation that was seen after carbohydrate plus protein ingestion. Phosphorylation of eNOS at Ser¹¹⁷⁷ is essential to insulin-mediated-NO production by endothelial cells ⁵⁴. Given that increases in insulin-mediated skeletal muscle perfusion are NO dependent ¹⁵, impaired eNOS Ser¹¹⁷⁷ phosphorylation may contribute to reduced glucose clearance following increased fat intake. Mechanistic support for the role of eNOS phosphorylation in enhancing skeletal muscle perfusion and glucose uptake comes from Kubota and colleagues ⁵⁵. In a series of elegant experiments, these authors demonstrated that impairments in insulin-mediated eNOS phosphorylation led to reduced skeletal muscle perfusion and impaired skeletal muscle glucose uptake. Moreover, restoration of insulin-mediated eNOS phosphorylation completely restored skeletal muscle perfusion and glucose uptake in mice lacking endothelial IRS-2 and those fed a high fat diet ⁵⁵. The possibility that impairments in insulin's microvascular action may be an early event in the development of lipid-induced insulin resistance is supported by recent animal work. Premilovac *et al.* ²² increased fat intake from 4.8% to 9.0% in Sprague Dawley rats and demonstrated that lipid-induced impairments in insulin-stimulated muscle glucose uptake originated solely from impairments in insulin's microvascular actions. In that study ²², the insulin sensitivity of the muscle fibers remained intact, which is in line with our observations in the present study. In contrast, animals fed a 22% fat diet experienced insulin resistance in both the microvasculature and the muscle fibers ²². Unlike the impairment in the insulin-induced activation of eNOS, high-fat overfeeding did not change the protein content of endothelial specific NOX2

(enzymatic subunit) and of p47phox (main regulator subunit) of NAD(P)H oxidase in skeletal muscle terminal arterioles and capillaries, suggesting that 7 days of high-fat overfeeding does not increase superoxide anion production by NAD(P)H oxidase.

As discussed above, the finding that 7 days of high-fat overfeeding impaired insulin-mediated eNOS phosphorylation in terminal arterioles could mean that a reduced ability to increase muscle perfusion in response to carbohydrate plus protein ingestion was responsible for reduced glucose clearance. However, we cannot be certain of this as we do not have a measure of muscle perfusion. It is also difficult to demonstrate causality in human experiments, and thus any observation of reduced muscle perfusion alongside impaired glucose clearance could be an epiphenomenon. Thus, further work is required to confirm whether dietary lipid-induced impairments in eNOS phosphorylation contribute to reduced glucose clearance. A further limitation of the present study is the lack of a control group maintaining their habitual diet. However, we had to consider the ethical correctness of including a separate control group that would undergo numerous muscle biopsies. For this reason, we chose to compare our experimental diet against our participant's habitual food intake, as we have done previously ⁴.

In conclusion, 7 days of high-fat overfeeding impaired whole-body glycemic control in healthy non-obese individuals. This was due to reduced glucose clearance, not elevated EGP. The reduction in glucose clearance occurred without an impairment in skeletal muscle insulin signaling, suggesting that an alternative mechanism is responsible for this effect of the high-fat diet. This study is the first to show that the insulin-induced Ser¹¹⁷⁷ phosphorylation of eNOS, which is known to lead to vasodilation of terminal arterioles after mixed meal ingestion, is impaired after 7 days of high-fat overfeeding. An additional strength of this study is the use of a carbohydrate-protein mixture to simultaneously create hyperglycemia and hyperinsulinemia,

which is more physiologically relevant than the clamp techniques that have been used in previous studies.

Data availability

The datasets generated during the current study are not publicly available but are available from the corresponding author on reasonable request.

References

1. Bray GA. Medical consequences of obesity. *The Journal of clinical endocrinology and metabolism*. 2004;89(6):2583-2589.
2. Hulston CJ, Churnside AA, Venables MC. Probiotic supplementation prevents high-fat, overfeeding-induced insulin resistance in human subjects. *The British journal of nutrition*. 2015;113(4):596-602.
3. Lundsgaard AM, Sjoberg KA, Hoeg LD, et al. Opposite Regulation of Insulin Sensitivity by Dietary Lipid Versus Carbohydrate Excess. *Diabetes*. 2017;66(10):2583-2595.
4. Parry SA, Smith JR, Corbett TR, Woods RM, Hulston CJ. Short-term, high-fat overfeeding impairs glycaemic control but does not alter gut hormone responses to a mixed meal tolerance test in healthy, normal-weight individuals. *The British journal of nutrition*. 2017;117(1):48-55.
5. Samuel VT, Shulman GI. The pathogenesis of insulin resistance: integrating signaling pathways and substrate flux. *The Journal of clinical investigation*. 2016;126(1):12-22.
6. Brons C, Jensen CB, Storgaard H, et al. Impact of short-term high-fat feeding on glucose and insulin metabolism in young healthy men. *The Journal of physiology*. 2009;587(Pt 10):2387-2397.
7. Kelley D, Mitrakou A, Marsh H, et al. Skeletal muscle glycolysis, oxidation, and storage of an oral glucose load. *The Journal of clinical investigation*. 1988;81(5):1563-1571.
8. DeFronzo RA. Pathogenesis of type 2 diabetes mellitus. *The Medical clinics of North America*. 2004;88(4):787-835, ix.

9. Kowalski GM, Bruce CR. The regulation of glucose metabolism: implications and considerations for the assessment of glucose homeostasis in rodents. *American journal of physiology Endocrinology and metabolism*. 2014;307(10):E859-871.
10. Jackson RA, Roshania RD, Hawa MI, Sim BM, DiSilvio L. Impact of glucose ingestion on hepatic and peripheral glucose metabolism in man: an analysis based on simultaneous use of the forearm and double isotope techniques. *The Journal of clinical endocrinology and metabolism*. 1986;63(3):541-549.
11. Barrett EJ, Wang H, Upchurch CT, Liu Z. Insulin regulates its own delivery to skeletal muscle by feed-forward actions on the vasculature. *American journal of physiology Endocrinology and metabolism*. 2011;301(2):E252-263.
12. Clerk LH, Vincent MA, Jahn LA, Liu Z, Lindner JR, Barrett EJ. Obesity blunts insulin-mediated microvascular recruitment in human forearm muscle. *Diabetes*. 2006;55(5):1436-1442.
13. Clerk LH, Vincent MA, Barrett EJ, Lankford MF, Lindner JR. Skeletal muscle capillary responses to insulin are abnormal in late-stage diabetes and are restored by angiotensin-converting enzyme inhibition. *American journal of physiology Endocrinology and metabolism*. 2007;293(6):E1804-1809.
14. Vincent MA, Clerk LH, Lindner JR, et al. Mixed meal and light exercise each recruit muscle capillaries in healthy humans. *American journal of physiology Endocrinology and metabolism*. 2006;290(6):E1191-1197.
15. Vincent MA, Barrett EJ, Lindner JR, Clark MG, Rattigan S. Inhibiting NOS blocks microvascular recruitment and blunts muscle glucose uptake in response to insulin. *American journal of physiology Endocrinology and metabolism*. 2003;285(1):E123-129.

16. Vincent MA, Clerk LH, Lindner JR, et al. Microvascular recruitment is an early insulin effect that regulates skeletal muscle glucose uptake in vivo. *Diabetes*. 2004;53(6):1418-1423.
17. Sjoberg KA, Frosig C, Kjobsted R, et al. Exercise Increases Human Skeletal Muscle Insulin Sensitivity via Coordinated Increases in Microvascular Perfusion and Molecular Signaling. *Diabetes*. 2017;66(6):1501-1510.
18. Natali A, Ribeiro R, Baldi S, et al. Systemic inhibition of nitric oxide synthesis in non-diabetic individuals produces a significant deterioration in glucose tolerance by increasing insulin clearance and inhibiting insulin secretion. *Diabetologia*. 2013;56(5):1183-1191.
19. Scherrer U, Randin D, Vollenweider P, Vollenweider L, Nicod P. Nitric oxide release accounts for insulin's vascular effects in humans. *The Journal of clinical investigation*. 1994;94(6):2511-2515.
20. Broussard JL, Castro AV, Iyer M, et al. Insulin access to skeletal muscle is impaired during the early stages of diet-induced obesity. *Obesity (Silver Spring, Md)*. 2016;24(9):1922-1928.
21. Olver TD, Grunewald ZI, Jurrissen TJ, et al. Microvascular insulin resistance in skeletal muscle and brain occurs early in the development of juvenile obesity in pigs. *American journal of physiology Regulatory, integrative and comparative physiology*. 2018;314(2):R252-r264.
22. Premilovac D, Bradley EA, Ng HL, Richards SM, Rattigan S, Keske MA. Muscle insulin resistance resulting from impaired microvascular insulin sensitivity in Sprague Dawley rats. *Cardiovascular research*. 2013;98(1):28-36.
23. Wagenmakers AJ, Strauss JA, Shepherd SO, Keske MA, Cocks M. Increased muscle blood supply and transendothelial nutrient and insulin transport induced by food intake

- and exercise: effect of obesity and ageing. *The Journal of physiology*. 2016;594(8):2207-2222.
24. Vincent MA, Montagnani M, Quon MJ. Molecular and physiologic actions of insulin related to production of nitric oxide in vascular endothelium. *Current diabetes reports*. 2003;3(4):279-288.
 25. Silver AE, Beske SD, Christou DD, et al. Overweight and obese humans demonstrate increased vascular endothelial NAD(P)H oxidase-p47(phox) expression and evidence of endothelial oxidative stress. *Circulation*. 2007;115(5):627-637.
 26. La Favor JD, Dubis GS, Yan H, et al. Microvascular Endothelial Dysfunction in Sedentary, Obese Humans Is Mediated by NADPH Oxidase: Influence of Exercise Training. *Arteriosclerosis, thrombosis, and vascular biology*. 2016;36(12):2412-2420.
 27. Mifflin MD, St Jeor ST, Hill LA, Scott BJ, Daugherty SA, Koh YO. A new predictive equation for resting energy expenditure in healthy individuals. *The American journal of clinical nutrition*. 1990;51(2):241-247.
 28. Borno A, Foged L, van Hall G. Glucose and glycerol concentrations and their tracer enrichment measurements using liquid chromatography tandem mass spectrometry. *Journal of mass spectrometry : JMS*. 2014;49(10):980-988.
 29. Hulston CJ, Woods RM, Dewhurst-Trigg R, et al. Resistance exercise stimulates mixed muscle protein synthesis in lean and obese young adults. *Physiological reports*. 2018;6(14):e13799.
 30. Cocks M, Shaw CS, Shepherd SO, et al. Sprint interval and endurance training are equally effective in increasing muscle microvascular density and eNOS content in sedentary males. *The Journal of physiology*. 2013;591(3):641-656.

31. Scott SN, Shepherd SO, Hopkins N, et al. Home-HIT improves muscle capillarisation and eNOS/NAD(P)H oxidase protein ratio in obese individuals with elevated cardiovascular disease risk. *The Journal of physiology*. 2019.
32. Wu F, Beard DA, Frisbee JC. Computational analyses of intravascular tracer washout reveal altered capillary-level flow distributions in obese Zucker rats. *The Journal of physiology*. 2011;589(Pt 18):4527-4543.
33. Knudsen SH, Karstoft K, Pedersen BK, van Hall G, Solomon TP. The immediate effects of a single bout of aerobic exercise on oral glucose tolerance across the glucose tolerance continuum. *Physiological reports*. 2014;2(8).
34. Camastra S, Muscelli E, Gastaldelli A, et al. Long-term effects of bariatric surgery on meal disposal and beta-cell function in diabetic and nondiabetic patients. *Diabetes*. 2013;62(11):3709-3717.
35. Ferrannini E, Muscelli E, Frascerra S, et al. Metabolic response to sodium-glucose cotransporter 2 inhibition in type 2 diabetic patients. *The Journal of clinical investigation*. 2014;124(2):499-508.
36. Matthews DR, Hosker JP, Rudenski AS, Naylor BA, Treacher DF, Turner RC. Homeostasis model assessment: insulin resistance and beta-cell function from fasting plasma glucose and insulin concentrations in man. *Diabetologia*. 1985;28(7):412-419.
37. Wang J, Obici S, Morgan K, Barzilai N, Feng Z, Rossetti L. Overfeeding rapidly induces leptin and insulin resistance. *Diabetes*. 2001;50(12):2786-2791.
38. Kim SP, Ellmerer M, Van Citters GW, Bergman RN. Primacy of hepatic insulin resistance in the development of the metabolic syndrome induced by an isocaloric moderate-fat diet in the dog. *Diabetes*. 2003;52(10):2453-2460.

39. Kraegen EW, Clark PW, Jenkins AB, Daley EA, Chisholm DJ, Storlien LH. Development of muscle insulin resistance after liver insulin resistance in high-fat-fed rats. *Diabetes*. 1991;40(11):1397-1403.
40. Kleemann R, van Erk M, Verschuren L, et al. Time-resolved and tissue-specific systems analysis of the pathogenesis of insulin resistance. *PloS one*. 2010;5(1):e8817.
41. Mevorach M, Giacca A, Aharon Y, Hawkins M, Shamoon H, Rossetti L. Regulation of endogenous glucose production by glucose per se is impaired in type 2 diabetes mellitus. *The Journal of clinical investigation*. 1998;102(4):744-753.
42. Bock G, Dalla Man C, Campioni M, et al. Pathogenesis of pre-diabetes: mechanisms of fasting and postprandial hyperglycemia in people with impaired fasting glucose and/or impaired glucose tolerance. *Diabetes*. 2006;55(12):3536-3549.
43. DeFronzo RA, Gunnarsson R, Bjorkman O, Olsson M, Wahren J. Effects of insulin on peripheral and splanchnic glucose metabolism in noninsulin-dependent (type II) diabetes mellitus. *The Journal of clinical investigation*. 1985;76(1):149-155.
44. Sano H, Kane S, Sano E, et al. Insulin-stimulated phosphorylation of a Rab GTPase-activating protein regulates GLUT4 translocation. *The Journal of biological chemistry*. 2003;278(17):14599-14602.
45. Zeigerer A, McBrayer MK, McGraw TE. Insulin stimulation of GLUT4 exocytosis, but not its inhibition of endocytosis, is dependent on RabGAP AS160. *Molecular biology of the cell*. 2004;15(10):4406-4415.
46. Miinea CP, Sano H, Kane S, et al. AS160, the Akt substrate regulating GLUT4 translocation, has a functional Rab GTPase-activating protein domain. *The Biochemical journal*. 2005;391(Pt 1):87-93.
47. Cartee GD. Roles of TBC1D1 and TBC1D4 in insulin- and exercise-stimulated glucose transport of skeletal muscle. *Diabetologia*. 2015;58(1):19-30.

48. Karlsson HK, Zierath JR, Kane S, Krook A, Lienhard GE, Wallberg-Henriksson H. Insulin-stimulated phosphorylation of the Akt substrate AS160 is impaired in skeletal muscle of type 2 diabetic subjects. *Diabetes*. 2005;54(6):1692-1697.
49. Tsintzas K, Chokkalingam K, Jewell K, Norton L, Macdonald IA, Constantin-Teodosiu D. Elevated free fatty acids attenuate the insulin-induced suppression of PDK4 gene expression in human skeletal muscle: potential role of intramuscular long-chain acyl-coenzyme A. *The Journal of clinical endocrinology and metabolism*. 2007;92(10):3967-3972.
50. Chokkalingam K, Jewell K, Norton L, et al. High-fat/low-carbohydrate diet reduces insulin-stimulated carbohydrate oxidation but stimulates nonoxidative glucose disposal in humans: An important role for skeletal muscle pyruvate dehydrogenase kinase 4. *The Journal of clinical endocrinology and metabolism*. 2007;92(1):284-292.
51. Mandarino LJ, Wright KS, Verity LS, et al. Effects of insulin infusion on human skeletal muscle pyruvate dehydrogenase, phosphofructokinase, and glycogen synthase. Evidence for their role in oxidative and nonoxidative glucose metabolism. *The Journal of clinical investigation*. 1987;80(3):655-663.
52. Constantin-Teodosiu D, Constantin D, Stephens F, Laithwaite D, Greenhaff PL. The role of FOXO and PPAR transcription factors in diet-mediated inhibition of PDC activation and carbohydrate oxidation during exercise in humans and the role of pharmacological activation of PDC in overriding these changes. *Diabetes*. 2012;61(5):1017-1024.
53. Constantin-Teodosiu D, Cederblad G, Bergstrom M, Greenhaff PL. Maximal-intensity exercise does not fully restore muscle pyruvate dehydrogenase complex activation after 3 days of high-fat dietary intake. *Clinical nutrition (Edinburgh, Scotland)*. 2018.

54. Montagnani M, Chen H, Barr VA, Quon MJ. Insulin-stimulated activation of eNOS is independent of Ca^{2+} but requires phosphorylation by Akt at Ser(1179). *The Journal of biological chemistry*. 2001;276(32):30392-30398.
55. Kubota T, Kubota N, Kumagai H, et al. Impaired insulin signaling in endothelial cells reduces insulin-induced glucose uptake by skeletal muscle. *Cell metabolism*. 2011;13(3):294-307.

Table and figure legends

Table 1. NEFA, non-esterified fatty acids; TAG, triacylglycerol; HDL, high-density lipoprotein cholesterol; LDL, low-density lipoprotein cholesterol; HOMA-IR, homeostatic model assessment of insulin resistance. Data presented are means \pm SEM ($n = 15$).

Figure 1. Plasma glucose (A) and serum insulin (B) before (pre) and after (post) 7 days of high-fat overfeeding. Time points -30 – 0 min represent the final 30 min of the 2-h pre-infusion period. All subsequent time points are following the ingestion of carbohydrate plus protein (indicated by dotted line). Data presented are means \pm SEM ($n = 15$). *significantly different between trials at the annotated time point ($P < 0.05$).

Figure 2. Endogenous glucose production (EGP) (A), oral glucose appearance (B), and whole-body glucose clearance rate (C) before (pre) and after (post) 7 days of high-fat overfeeding. Time points -30 – 0 min represent the final 30 min of the initial 2-h pre-infusion period. All subsequent time points are following ingestion of carbohydrate plus protein (indicated by dotted line). Data presented are means \pm SEM ($n = 14$).

Figure 3. Phosphorylation of skeletal muscle Akt Ser⁴⁷³ (A), Akt Thr³⁰⁸ (B), AS160 Ser⁵⁸⁸ (C), and AS160 Thr⁶⁴² (D) during fasting and following ingestion of carbohydrate plus protein, before (pre) and after (post) 7 days of high-fat overfeeding. Data presented are means \pm SEM ($n = 13$). AU, arbitrary units. †significantly higher than 0 min ($P < 0.05$). ‡significantly lower than 30 min ($P < 0.05$).

Figure 4. eNOS content in terminal arterioles and capillaries before (pre) and after (post) 7 days of high-fat overfeeding. A, representative confocal microscopy images of skeletal muscle

arterioles from pre- (a) and post-high-fat overfeeding (b). The skeletal muscle microvascular endothelium was revealed using Ulex europaeus-FITC conjugated lectin (UEA-I) (green). Skeletal muscle eNOS expression was revealed using Alexa Fluor 546 conjugated secondary antibody (red). Images not shown, arterioles and capillaries were differentiated using anti- α smooth muscle actin in combination with Alexa Fluor 405 conjugated secondary antibody. Bar represents 10 μ m. B, mean fluorescence intensity of eNOS is summarized. Data presented as means \pm SEM ($n = 12$). *Significantly lower than before high-fat overfeeding ($P < 0.05$).

Figure 5. eNOS phosphorylation in terminal arterioles and capillaries during fasting (0 min) and 30 min after consuming carbohydrate plus protein, before (pre) and after (post) 7 days of high-fat overfeeding. A and B, representative confocal microscopy images of skeletal muscle arterioles from pre- (A) and post-high-fat overfeeding (B), in the fasted (a) and stimulated (b) state. The skeletal muscle microvascular endothelium was revealed using Ulex europaeus-FITC conjugated lectin (UEA-I) (green). Skeletal muscle eNOS Ser¹¹⁷⁷ phosphorylation was revealed using Alexa Fluor 633 conjugated secondary antibody (red). Images not shown, arterioles and capillaries were differentiated using anti- α smooth muscle actin in combination with Alexa Fluor 405 conjugated secondary antibody. Bar represents 10 μ m. C, mean fluorescence intensity of eNOS Ser¹¹⁷⁷ is summarized. D, eNOS Ser¹¹⁷⁷ phosphorylation normalized to eNOS content. Data presented as means \pm SEM ($n = 12$). †Significant increase from 0 min (fasted) ($P < 0.05$).

Figure 6. NOX2 and p47phox content in terminal arterioles and capillaries before (pre) and after (post) 7 days of high-fat overfeeding. A and B, representative confocal microscopy images of skeletal muscle from pre- (a) and post-high-fat overfeeding (b), illustrating NOX2 (A) and p47phox (B). The skeletal muscle microvascular endothelium was revealed using Ulex

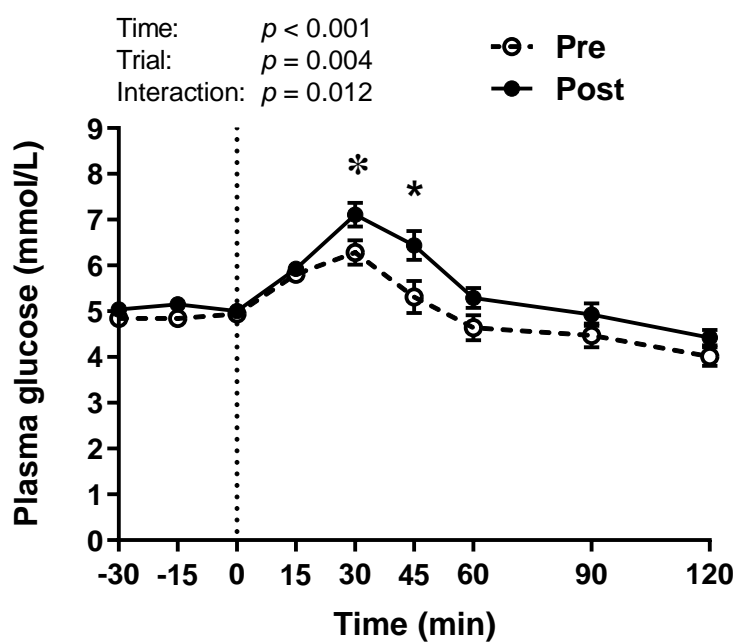
europaeus-FITC conjugated lectin (UEA-I) (green). Skeletal muscle NOX2 and p47phox expression were revealed using an Alexa Fluor 546 conjugated secondary antibody (red). Images not shown, arterioles and capillaries were differentiated using anti- α smooth muscle actin in combination with Alexa Fluor 405 conjugated secondary antibody. Bar represents 25 μ m. C, mean fluorescence intensity of NOX2 is summarized. D, mean fluorescence intensity of p47phox is summarized. Data presented as means \pm SEM (n = 12).

Table 1. Body mass, fasting biochemical blood parameters, and HOMA-IR before (pre) and after (post) 7-days of high-fat overfeeding

	Pre	Post	Significance
Body mass (kg)	77.65 ± 3.02	78.97 ± 3.06	<i>P</i> < 0.001
Glucose (mmol/L)	4.87 ± 0.08	5.06 ± 0.08	<i>P</i> = 0.027
Insulin (pmol/L)	67 ± 6	80 ± 7	<i>P</i> = 0.019
NEFA (mmol/L)	0.56 ± 0.08	0.35 ± 0.04	<i>P</i> = 0.003
TAG (mmol/L)	0.82 ± 0.07	0.60 ± 0.06	<i>P</i> < 0.001
Total cholesterol (mmol/L)	3.75 ± 0.15	3.88 ± 0.12	<i>P</i> = 0.034
HDL (mmol/L)	1.32 ± 0.08	1.56 ± 0.08	<i>P</i> < 0.001
LDL (mmol/L)	2.16 ± 0.14	2.06 ± 0.14	<i>P</i> = 0.113
HOMA-IR	2.1 ± 0.2	2.6 ± 0.2	<i>P</i> = 0.011

Figure 1

A



B

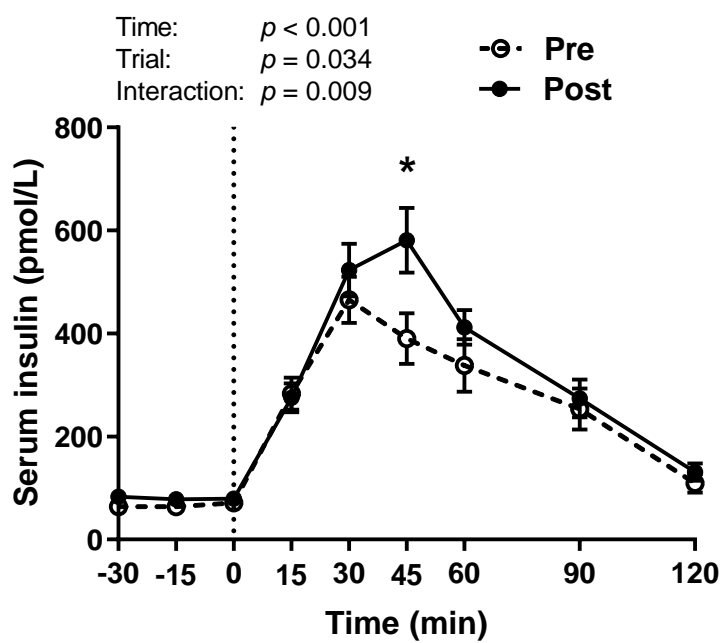


Figure 2

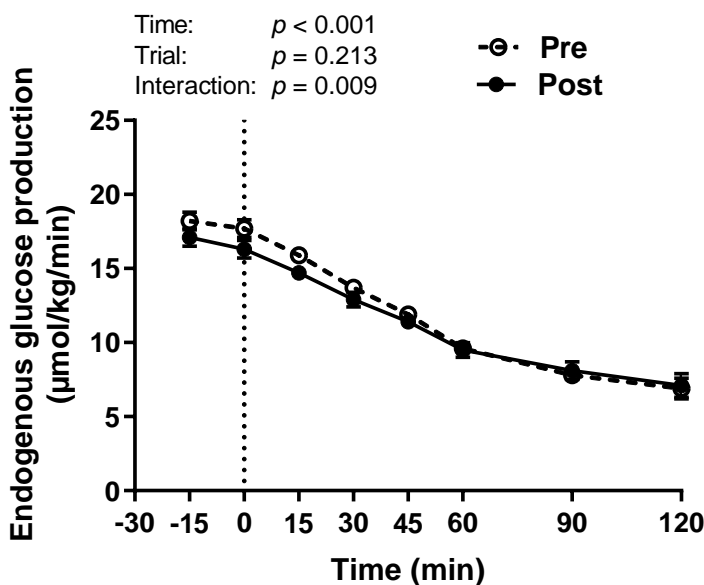
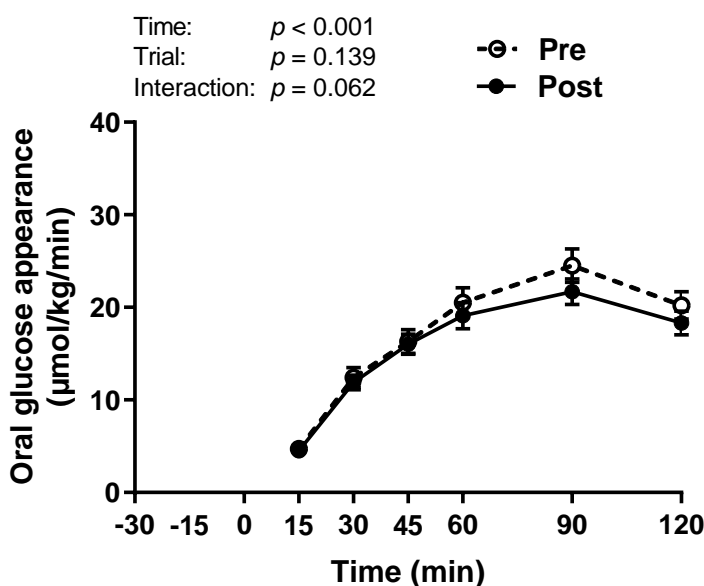
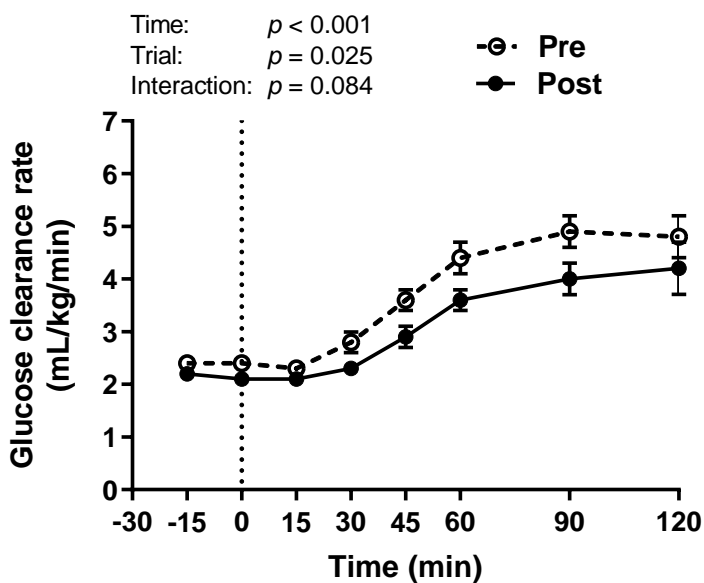
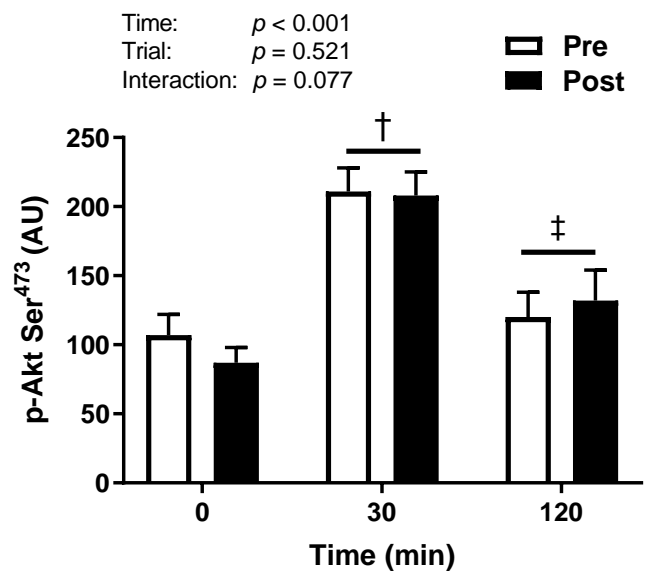
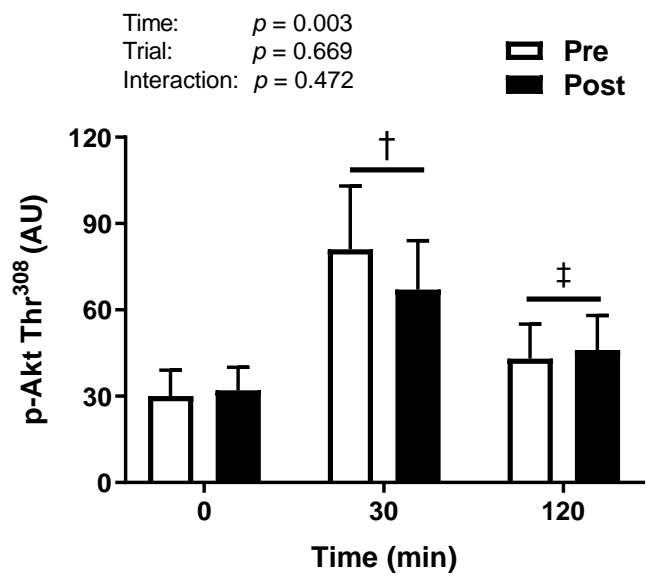
A**B****C**

Figure 3

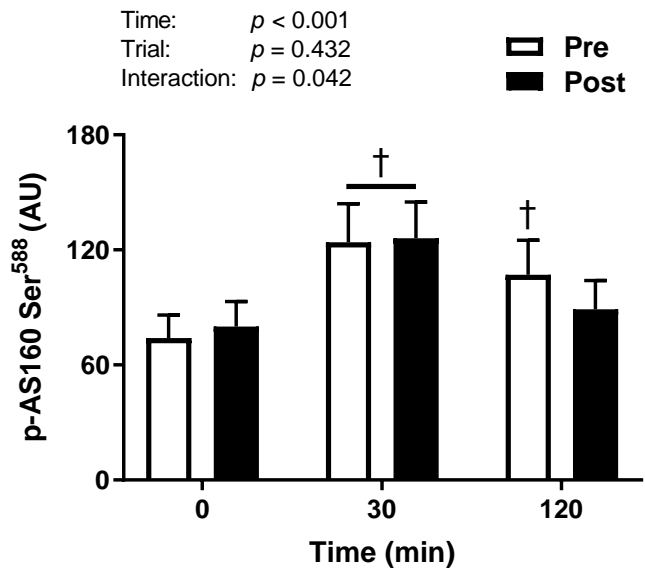
A



B



C



D

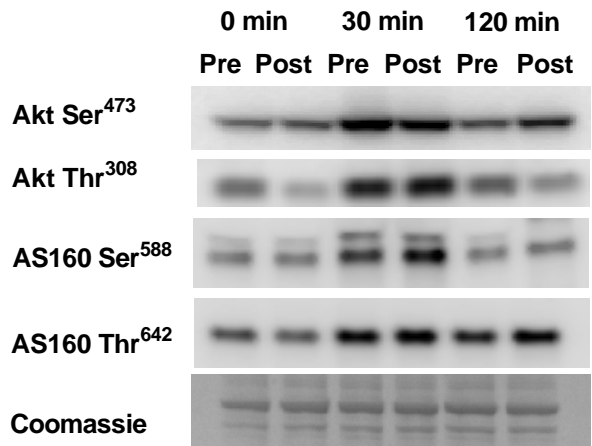
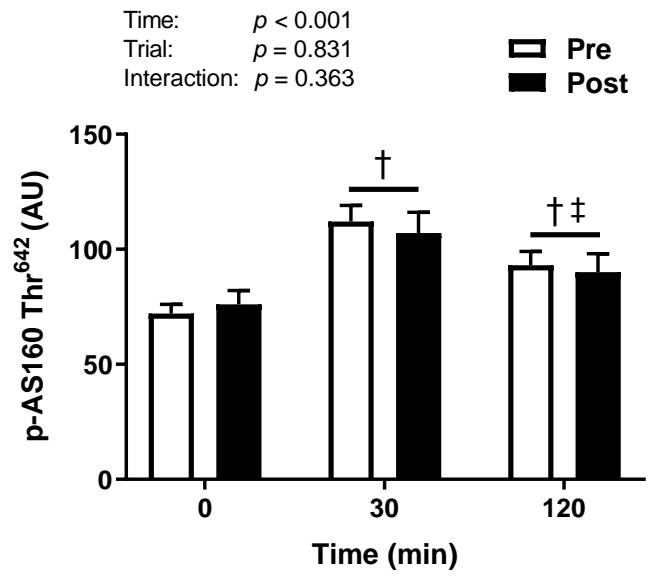
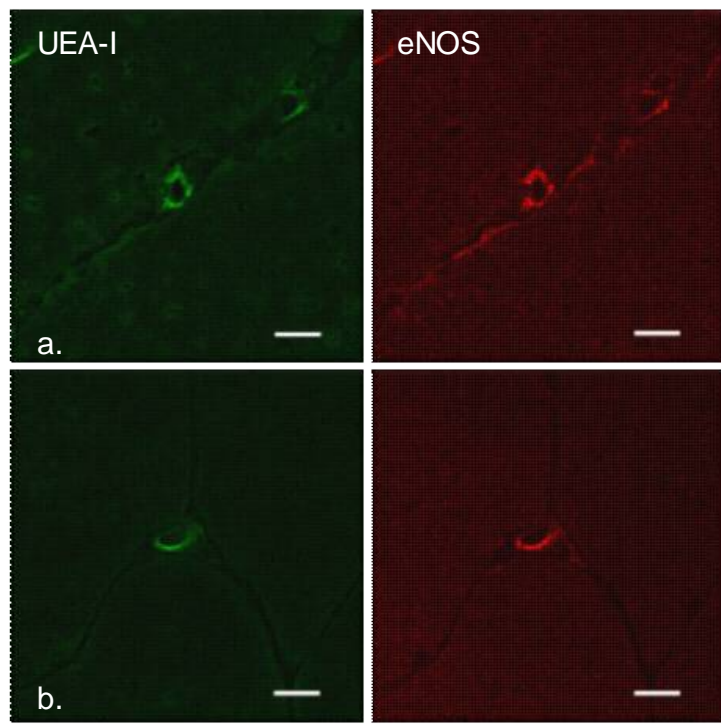


Figure 4

A



B

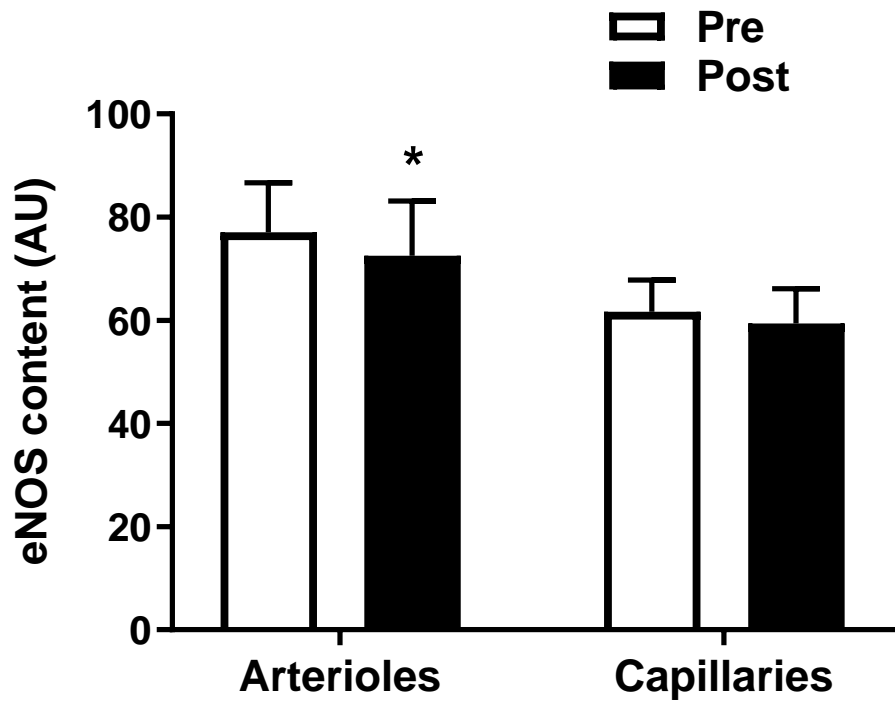
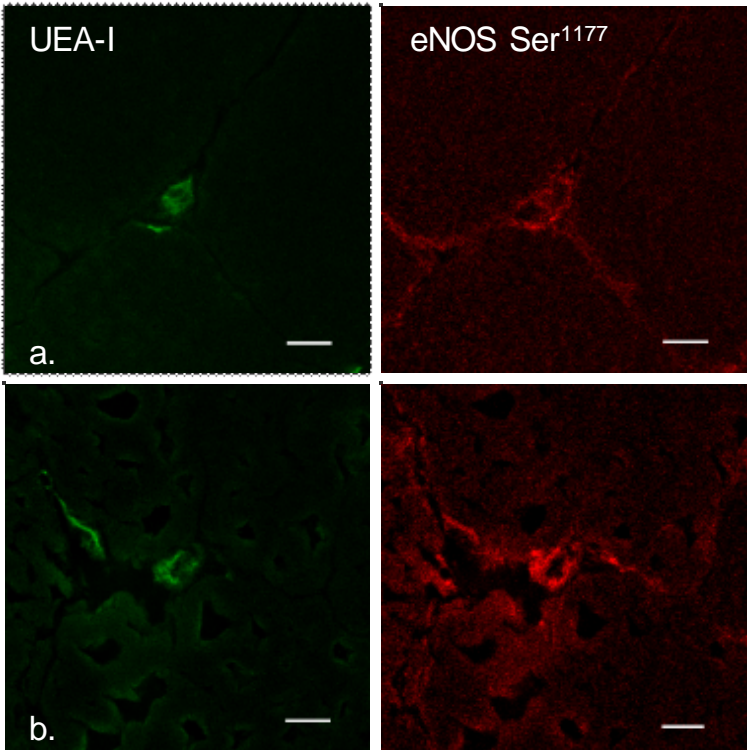
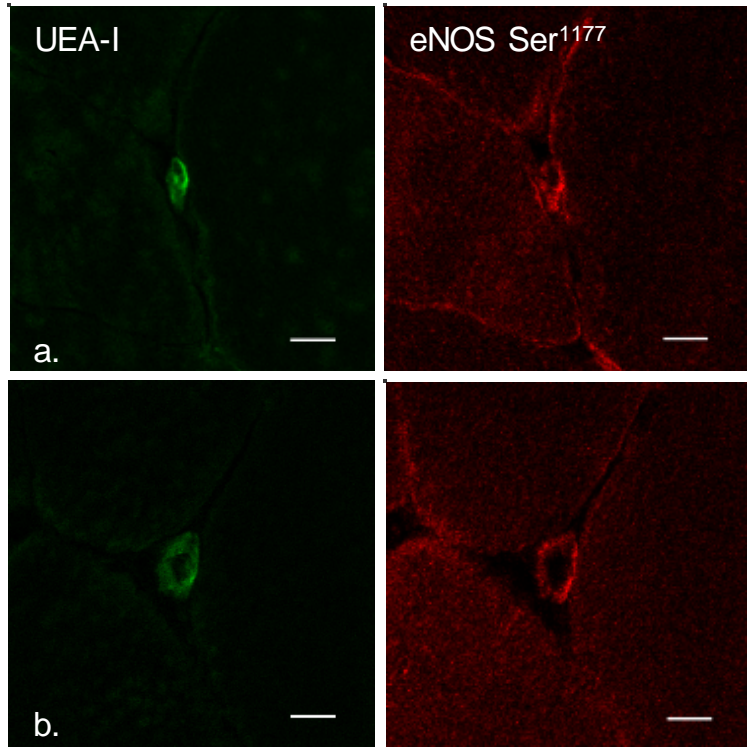


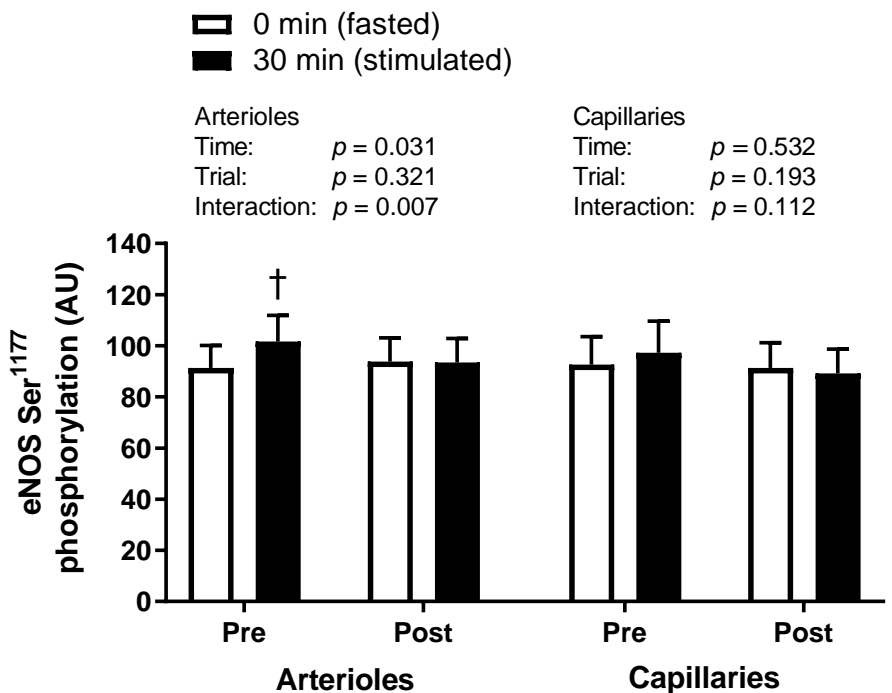
Figure 5
A



B



C



D

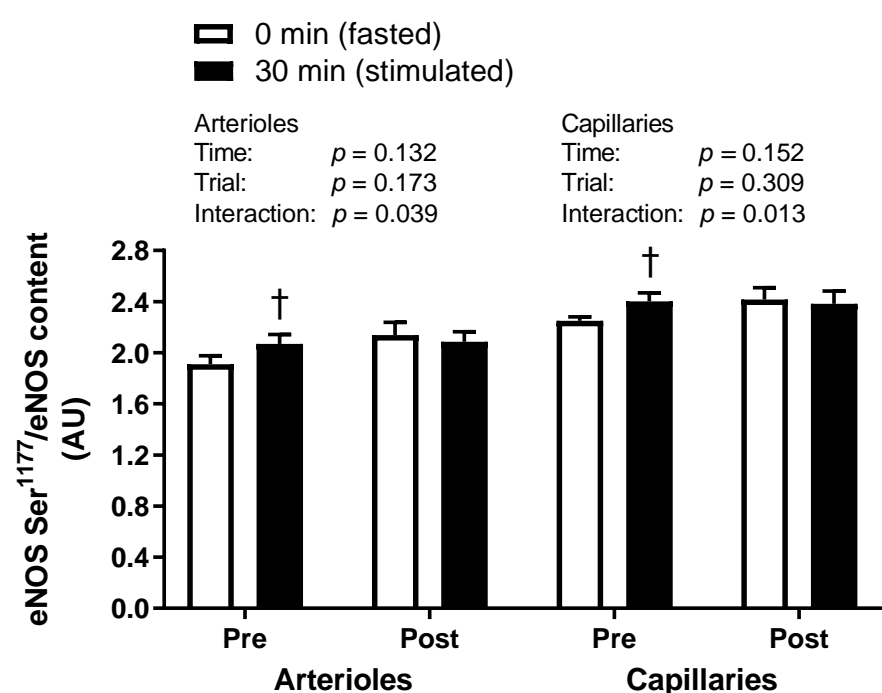
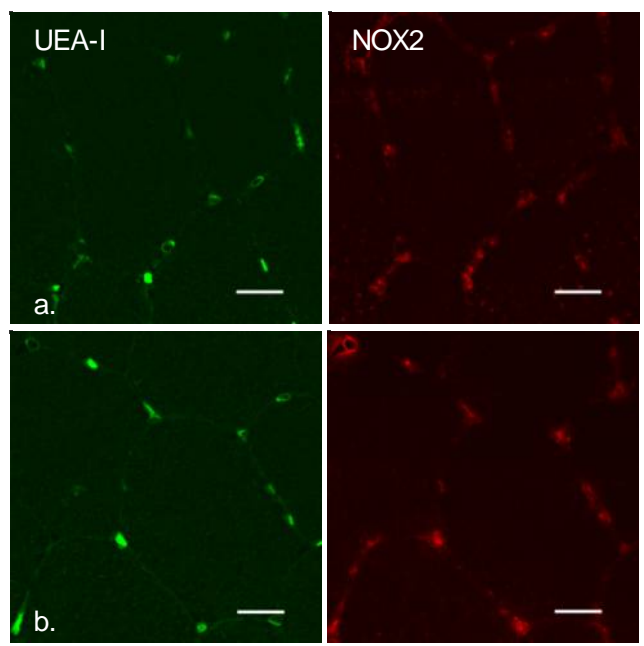
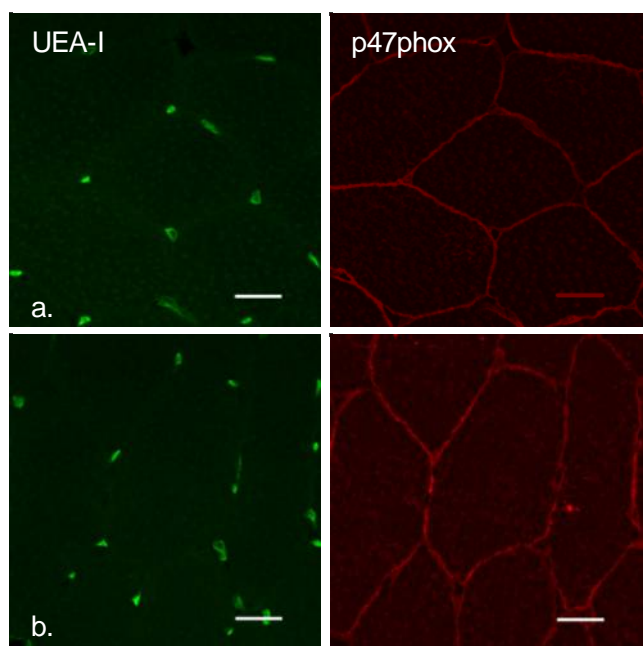


Figure 6

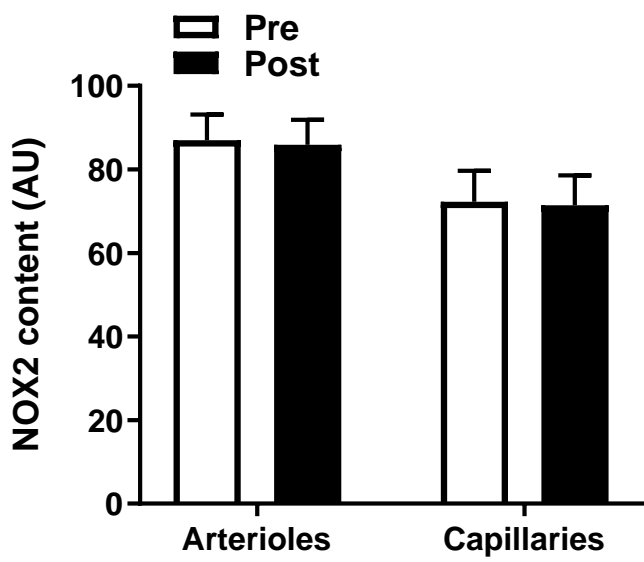
A



B



C



D

